Combustion Theory and Modelling
Vol. 13, No. 2, 2009, 269–294

Generalized flame balls

Joel Daou[1,*], Faisal Al-Malki[1] and Paul Ronney[2]

[1] *School of Mathematics, University of Manchester, Manchester M13 9PL, UK;*
[2] *Department of Aerospace and Mechanical Engineering, University of Southern California, Los Angeles, CA 90089-1453, USA*

(*Received 10 June 2008; final version received 20 October 2008*)

We consider *generalized flame balls* which correspond to stationary spherical flames with a flow of hot inert gas, either a source or a sink, at the origin. Depending on the flow, these flames can have positive, zero, or negative burning speeds, with zero speeds characterizing the Zeldovich flame balls. A full analytical description of these structures and their stability to radial perturbations is provided, using a large activation energy asymptotic approach and a thermo-diffusive approximation. The results are also complemented by a numerical study. The number and stability of the generalized flame balls are identified in various regions of the l-M-h_0 space, where l is the (reduced) Lewis number, and M and h_0 the flow rate and its enthalpy at the origin, respectively. It is typically found that, when the flow is a source, there is a maximum value of the flow rate $M_{\max}$ depending on l and h_0, above which no stationary solutions exist, and below which there are two solutions characterizing a small stable flame ball and a large unstable flame ball; the implications of these results to the problem of ignition by a hot inert gas stream are discussed. When the flow is a sink, however, there is typically a single unstable solution, except for sufficiently large values of the Lewis number and large negative values of M, where three flame balls exist, the medium one being stable. Finally, the relation between the flame speed, positive or negative, and the flame curvature, small or large, is discussed.

Keywords: flame balls; ignition by a hot stream; flame stability

1. Introduction

Flame balls are non-propagating spherical flames, predicted by Zeldovich over sixty years ago, as stationary solutions of the heat conduction and diffusion equations in a motionless reactive mixture [1, p. 327]. These solutions are unstable under adiabatic conditions [1, p. 331], [2]. However, theoretical studies have shown that flame balls may be stabilized if account is taken of additional physical mechanisms such as volumetric heat-loss [3, 4], conductive heat-loss to walls [5] or suitably defined weakly non-uniform flow fields [6]. In these studies, two branches of solutions are typically found when the radius of the flame balls is plotted versus a control parameter such as the intensity of volumetric heat-loss, smaller than a critical value; the solutions on the lower branch representing small flames including Zeldovich flame balls are unstable, while those on the upper branch representing large flame balls are stable for a given range of the control parameter. In fact, much of the recent theoretical work on flame balls has been motivated by the observation of such

*Corresponding author. Email: joel.daou@manchester.ac.uk

ISSN: 1364-7830 print / 1741-3559 online

DOI: 10.1080/13647830802596447
http://www.tandf.co.uk/journals

apparently stable structures in lean hydrogen–air mixtures in the experiments by Ronney and coworkers under micro-gravity conditions [7, 8].

In addition to the significance of flame balls as a possible mode of combustion in weakly flammable mixtures, an important related aspect, of particular relevance to the present work, is their significance in ignition problems involving heat addition by an external source such as an electric spark. In this context, they may indeed serve to estimate the minimum energy to be deposited by the source for successful ignition whereby an initially formed hot kernel generates an outwardly propagating flame front [1, p. 331]. For successful ignition to occur, however, both the power and the duration of the source need be taken into account [2, 9, 10]. In the particular case of a point source of constant power, two branches of stationary solutions are obtained depending on the power of the source [2]; the lower branch representing small flame balls which are stable, the upper branch representing large flame balls, including Zeldovich flame balls, which are unstable.

In this work, we extend these studies, by considering a model for flame balls in the presence of a flow of hot inert gas, either a source or a sink, at their origin. Depending on the direction and magnitude of the flow, these flames can have positive, zero or negative burning speeds, with zero speeds characterizing Zeldovich flame balls. We shall refer to these stationary solutions of the advection-diffusion-reaction heat and mass transport equations as *generalized flame balls*.

One motivation for studying these solutions is that they provide a simple framework for analysing the important problem of flame initiation, intentional or accidental, by a hot gas stream; [11, p. 265] and [12]. They also provide valuable analytical information on the effect of convection, albeit for a specific radial flow, on the existence and stability of flame balls. Finally, the dependence of their burning velocity, positive or negative, on their curvature, small or large, may provide some insight into such dependence when studying the local behaviour of more complex premixed flames such as edge-flames in strained mixing layers or flamelets in turbulent flow fields.

The paper is structured as follows. We begin by formulating the model and identifying its main non-dimensional parameters. An asymptotic analysis is then presented, where the stationary solutions, their multiplicity and their stability are fully described. This is followed by a numerical study which validates and illustrates the analytical results. Finally, a conclusion section where the main findings are summarized and additional extensions of the work suggested, closes the paper.

2. Formulation

We consider a spherically symmetric flame around a point source of hot inert gas located at the origin, as shown in Figure 1. Within the thermo-diffusive approximation of constant density and constant transport properties, a relevant non-dimensional model consists of the equations

$$\frac{\partial \theta}{\partial t} + \frac{M}{r^2}\frac{\partial \theta}{\partial r} = \frac{1}{r^2}\frac{\partial}{\partial r}\left(r^2 \frac{\partial \theta}{\partial r}\right) + \omega, \tag{1}$$

$$\frac{\partial y_F}{\partial t} + \frac{M}{r^2}\frac{\partial y_F}{\partial r} = \frac{1}{\mathrm{Le}}\frac{1}{r^2}\frac{\partial}{\partial r}\left(r^2 \frac{\partial y_F}{\partial r}\right) - \omega, \tag{2}$$

subject to the far-field boundary condition

$$\theta = 0, \qquad y_F = 1 \qquad \text{as} \quad r \to \infty, \tag{3}$$

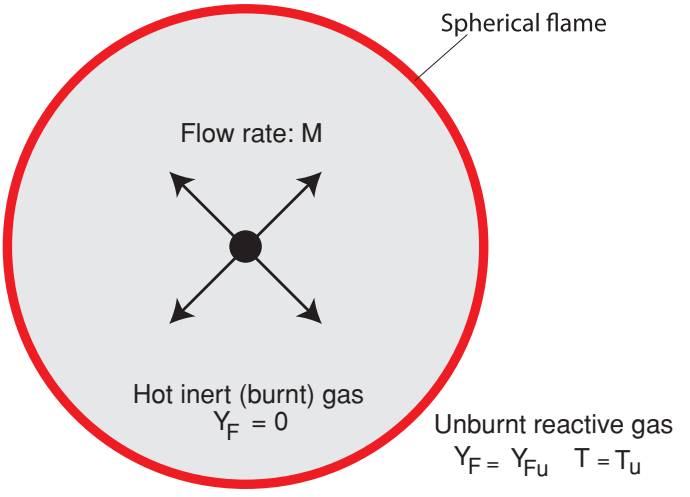

Figure 1. Spherical flame sustained by a point source of hot inert gas, with flow rate $M > 0$. Negative values of M correspond to a sink (not shown in this figure).

and the requirement inside the ball that

$$\begin{cases} (\theta, y_F) = (\theta_0, 0) & \text{for} \quad M > 0 \\ \\ (\theta, y_F) \text{ are bounded} & \text{for} \quad M \leq 0 \end{cases} \quad \text{as} \quad r \to 0\,. \tag{4}$$

Here θ and y_F are the non-dimensional temperature and mass fraction of the fuel, respectively, and Le is the Lewis number. They are given by $\theta = (T - T_u)/(T_{ad} - T_u)$ and $y_F = Y_F/Y_{Fu}$, where T_u and Y_{Fu} are the temperature and the fuel mass fraction of the reactive mixture in the far-field, and T_{ad} is the adiabatic *planar flame* temperature. The fuel is assumed to limit the reaction rate ω, which is taken to follow the standard (non-dimensional) Arrhenius form

$$\omega = \frac{\beta^2}{2\mathrm{Le}} y_F \exp\left(\frac{\beta(\theta - 1)}{1 + \alpha(\theta - 1)}\right),$$

where β is the non-dimensional activation energy or Zeldovich number, and $\alpha = (T_{ad} - T_u)/T_{ad}$ the heat release parameter. A convection term of strength M is included in the equations to account for the presence of a point-source radial flow at the origin if $M > 0$, where M represents the non-dimensional volumetric flow rate; when $M < 0$, we are in the presence of a sink which sucks the burnt gas. The units for speed and length chosen for the non-dimensionalization correspond to the propagation speed S_L and the thickness δ_L of the *planar flame* (more precisely to the asymptotic values of these as $\beta \to \infty$).

The far-field boundary condition (3) corresponds to a frozen mixture with prescribed temperature and composition. The boundary condition (4) specifies the temperature of the fuel-free (inert) stream at the origin when $M > 0$; when $M \leq 0$, θ and y_F are simply required to be bounded.

We have now completed the formulation of the problem. The main task is to find time-independent solutions to Equations (1)–(4) which represent spherical flame balls whose radius R depend on the parameters Le, M and θ_0, in addition to β and α.

We begin by reformulating the problem in the asymptotic limit $\beta \to \infty$ in the next section. This is followed by an analytical treatment which allows R to be determined in terms of three parameters representing Le, M and θ_0, along with the multiplicity of the solutions. The linear stability of these to one-dimensional perturbations is then addressed analytically. Finally, a numerical treatment of the problem with a finite value of β is provided, which supports and illustrates the analytical findings. We also discuss the application of the results to the problem of ignition by a hot inert gas flow and to clarifying the dependence of the speed and the burning rate of the flames encountered on their curvatures.

3. The large activation energy asymptotic limit

In the limit $\beta \to \infty$, the reaction is confined to an infinitely thin reaction sheet, located at $r = r_f$, say. It is convenient to adopt the near-equidiffusion flame (NEF) approximation for which $l \equiv \beta(\mathrm{Le} - 1)$ is $\mathcal{O}(1)$, supplemented by the assumption that the temperature at the origin θ_0 may deviate from unity by an amount at most of $\mathcal{O}(\beta^{-1})$, and thus may be written as $\theta_0 = 1 + h_0/\beta$, which defines h_0. These assumptions insure that the leading order temperature θ^0 is unity in the burnt gas, $\theta^0(r \le r_f) = 1$, and allow the problem to be reformulated in terms of θ^0 and the (excess) enthalpy $h \equiv \theta^1 + y_F^1 \sim \beta(\theta + y_F - 1)$; see e.g. [13, p. 38] and [14]. Here and below superscripts indicate expansions in terms of β^{-1}. In terms of θ^0 and h we have to solve

$$\frac{\partial \theta^0}{\partial t} + \frac{M}{r^2}\frac{\partial \theta^0}{\partial r} = \frac{1}{r^2}\frac{\partial}{\partial r}\left(r^2 \frac{\partial \theta^0}{\partial r}\right) \qquad (r > r_f) \tag{5}$$

$$\frac{\partial h}{\partial t} + \frac{M}{r^2}\frac{\partial h}{\partial r} = \frac{1}{r^2}\frac{\partial}{\partial r}\left(r^2 \frac{\partial h}{\partial r}\right) + \frac{l}{r^2}\frac{\partial}{\partial r}\left(r^2 \frac{\partial \theta^0}{\partial r}\right) \qquad (r \neq r_f) \tag{6}$$

subject to the far-field boundary condition

$$\theta^0 = 0, \qquad h = 0 \qquad \text{as} \quad r \to \infty \tag{7}$$

and the requirement inside the ball that

$$\begin{cases} h = h_0 & \text{for} \quad M > 0 \\ h \text{ is bounded} & \text{for} \quad M \le 0 \end{cases} \qquad \text{as} \quad r \to 0\,. \tag{8}$$

In addition, the jump conditions

$$[\theta^0] = 0, \quad [h] = 0\,, \tag{9a}$$

$$\left[\frac{\partial h}{\partial r}\right] + l\left[\frac{\partial \theta^0}{\partial r}\right] = 0\,, \tag{9b}$$

$$\left[\frac{\partial \theta^0}{\partial r}\right] = \exp\left(\frac{h(r_f^-)}{2}\right), \tag{9c}$$

must be satisfied; here $[\quad] = (\quad)_{r_f^-} - (\quad)_{r_f^+}$, indicate a jump at the reaction sheet located at $r = r_f$ (see e.g. [13, p. 39] and [15, p. 529]).

4. Analytical results

In this section, we consider the problem described by Equations (5)–(9). We thus have three free parameters, namely, M (the flow rate), l (the reduced Lewis number), and h_0 (the excess enthalpy at the origin).

4.1. *The stationary profiles*

Stationary solutions satisfying (5)–(9), except the last jump condition 9c, are readily determined, and are given by

$$\theta^0 = \begin{cases} 1 & \text{for} \quad r \le R \\ \frac{1-e^{-M/r}}{1-e^{-M/R}} & \text{for} \quad r \ge R \end{cases} \tag{10}$$

$$h = \begin{cases} h_* + H(M)\,(h_0 - h_*)\left[1 - \frac{e^{-M/r}}{e^{-M/R}}\right] & \text{for} \quad r \le R \\ \left[h_* + \frac{lM}{R} \cdot \frac{e^{-M/R}}{1-e^{-M/R}}\right] \frac{1-e^{-M/r}}{1-e^{-M/R}} - \frac{lM}{r} \frac{e^{-M/r}}{1-e^{-M/R}} & \text{for} \quad r \ge R \end{cases} \tag{11}$$

where $h_* \equiv h(R)$, characterizing the departure of the flame temperature from the adiabatic planar flame value, is given by

$$h_* \equiv h(R) = -\frac{lM}{R(1-e^{-M/R})} + H(M)\left[h_0(1-e^{-M/R}) + \frac{lM}{R}\right] \tag{12}$$

and $H(M)$ is the Heaviside function defined by

$$H(M) = \begin{cases} 0 & \text{for} \quad M \le 0 \\ 1 & \text{for} \quad M > 0\,. \end{cases}$$

On using the remaining jump condition (9c), we obtain

$$\frac{M}{R^2} \frac{e^{-M/R}}{1-e^{-M/R}} = \exp\left(\frac{h_*}{2}\right),$$

i.e.

$$\frac{M}{R^2} \frac{e^{-M/R}}{1-e^{-M/R}} = \exp\left(-\frac{lM}{2R(1-e^{-M/R})} + H(M)\left[\frac{h_0}{2}(1-e^{-M/R}) + \frac{lM}{2R}\right]\right), \tag{13}$$

which allows the radius of the stationary flame R to be determined in terms of M, l, and h_0.

It can be noted that when $M \leq 0$ the enthalpy h inside the ball is a constant equal to $h_* \equiv h(R)$ which is determined as part of the solution and is independent of the choice of h_0. In contrast, when $M > 0$ corresponding to a source at the origin, h_0 is of course essential in determining the profiles.

4.2. *Notation and preliminary remarks*

In order to facilitate the discussion of the results, we introduce here two quantities μ and S characterizing the flame by

$$\mu = \exp\left(\frac{h_*}{2}\right) \quad \text{(burning rate)} \tag{14}$$

and

$$S = -\frac{M}{R^2} \quad \text{(flame speed)}. \tag{15}$$

The quantity μ represents the (non-dimensional) burning rate per unit flame area, a fact which follows from the jump condition (9c).[1] It is equal here to each side of Equation (13).

The quantity S represents the flame speed or burning velocity defined as the speed with which the flame travels with respect to the unburnt gas ahead of it (or more precisely just ahead of its reaction sheet[2]), or equivalently, as minus the speed of the unburnt gas at $r = R^+$ with respect to the stationary flame ball, this speed being obviously given by the right-hand side of (15). It can be noted therefore that negative flame speeds S are obtained for $M > 0$, and positive flame speeds for $M < 0$.

We note that Equation (12) can be written as

$$h_* = -\frac{lm}{1 - e^{-m}} + H(m)\left[h_0(1 - e^{-m}) + lm\right] \tag{16}$$

showing that the perturbation in the flame temperature h_* is a function of the parameter $m \equiv M/R$, in addition to the reduced Lewis number l and the excess enthalpy h_0; $h_* = h_*(m; l, h_0)$. Also, Equation (13) can be recast into the parametric form

$$R = R(m; l, h_0) = \frac{m \exp\left(\frac{l}{2}\frac{m}{1-e^{-m}} - H(m)\left[\frac{h_0}{2}(1 - e^{-m}) + \frac{lm}{2}\right]\right)}{e^m - 1} \tag{17a}$$

$$M = M(m; l, h_0) = mR(m; l, h_0)\,, \tag{17b}$$

involving the parameter m. Parametric plots of R versus M, and similarly of $S = -M/R^2 = -m/R$ and μ versus M, can thus be generated by varying m in the range $(-\infty, \infty)$ for selected fixed values of l and h_0. For future reference we record the asymptotic behaviour

$$R \sim -m\,, \quad M \sim -m^2\,, \quad \mu \sim 1\,, \quad S \sim 1 \quad as \quad m \to -\infty\,, \tag{18}$$

[1] Indeed, since $\theta^0 + y_F^0 = 1$ everywhere, and $y_F = 0$ in the burnt gas, the left-hand side of (9c) reduces to $(\partial y_F^0/\partial r)_{r=r_f^+}$, which is the (non-dimensional) mass of fuel reaching the reaction sheet per unit area of the latter and unit time, in the limit $\beta \to \infty$.

[2] Using the location of the reaction sheet to define the flame speed is a convenient and unambiguous choice in the limit $\beta \to \infty$, although other choices are possible [16].

which follows from (14) to (17). This shows that in the limit of infinitely strong sink, $M \to -\infty$, the radius of the stationary flame is large, $R \sim \sqrt{-M}$, while its burning rate μ and speed S approach those of the planar flame as expected. On the other hand, we have

$$R \sim me^{-m-\frac{h_0}{2}},\ M \sim m^2 e^{-m-\frac{h_0}{2}},\ \mu \sim e^{\frac{h_0}{2}},\ S \sim -e^{m+\frac{h_0}{2}} \quad as \quad m \to \infty, \tag{19}$$

so that, in particular, $R \to 0$ and $M \to 0$ as $m \to \infty$; this shows that all curves of R versus M must approach the point ($R = 0$, $M = 0$) and that S takes infinitely large negative values in this limit.

4.3. *The adiabatic case $h_0 = 0$*

We begin with the adiabatic case $h_0 = 0$, whose results are summarized in Figure 4.3. Plotted versus M are the flame radius R (top), the flame speed S (middle) and the burning rate per unit flame area μ (bottom), for selected values of l. These curves are generated as parametric plots, as explained in the previous paragraph, by varying the parameter m in the range $(-\infty, \infty)$; for illustration, an arrow has been added to the curve R versus M corresponding to $l = 0$ to indicate the direction of increasing m. It is observed that a maximum value of M depending on l exists, say $M_{\max}$, above which there are no stationary solutions. As will be demonstrated later, $M_{\max}$ defines in fact a critical value of M for ignition to occur, with ignition defined as the transition from stationary to outwardly propagating flames.

For $0 \le M < M_{\max}$, each curve R versus M has two branches of solutions, representing flame balls with burning speeds $S \le 0$. The upper branch intersects the vertical axis, $M = 0$, at a value of R corresponding to Zeldovich flame balls,[3] $R = \exp(l/2)$, as can be verified by taking the limit $m \to 0$ in (17). For solutions on this upper branch, R and S are decreasing functions of M, and so is μ if $l < 0$; μ is an increasing function of M if $l > 0$, and constant equal to one if $l = 0$. The lower branch intersects the vertical axis at the point ($R = 0$, $M = 0$), in agreement with the asymptotic behaviour 19 obtained for $m \to \infty$; in this limit we have also $S \to -\infty$, and, in the present case with $h_0 = 0$, $\mu \to 1$. For solutions on this lower branch, R and S are increasing functions of M, and so is μ if $l < 0$; μ is a decreasing function of M if $l > 0$, and $\mu = 1$ if $l = 0$.

For $M < 0$, we have typically a unique solution, that is a single-valued dependence of R on M, as exemplified in the cases $l = -2$, $l = 0$ and $l = 2$. As $M \to -\infty$, and irrespective of the value of l, the flame is rejected to infinity, and therefore behaves as a planar flame, in conformity with the asymptotic formulae (18) obtained in the limit $m \to -\infty$. It is notable however that this uniqueness of solution is lost when l is sufficiently large, as illustrated in the case $l = 8$ for which R versus M takes the form of an S-shaped curve, for $M < 0$.

It is instructive to determine in the l-M plane the locus of the turning points of the S-shaped curve obtained for $M < 0$ and of the maximum flow rate $M_{\max}$. At these points, we must have $dM/dm = 0$, which can be solved for l to yield a relation of the form $l = l(m; h_0)$, namely,

$$l = \begin{cases} \dfrac{4e^{-2m} + (2m-8)e^{-m} - 2m + 4}{m(me^{-m} + e^{-m} - 1)} & (m < 0) \\ \dfrac{\left[(e^{-m}-1)(4 - me^{-m}h_0) + 2m\right](e^{-m}-1)}{me^{-m}(e^{-m} + m - 1)} & (m > 0). \end{cases} \tag{20}$$

[3] See e.g. [15, p. 530].

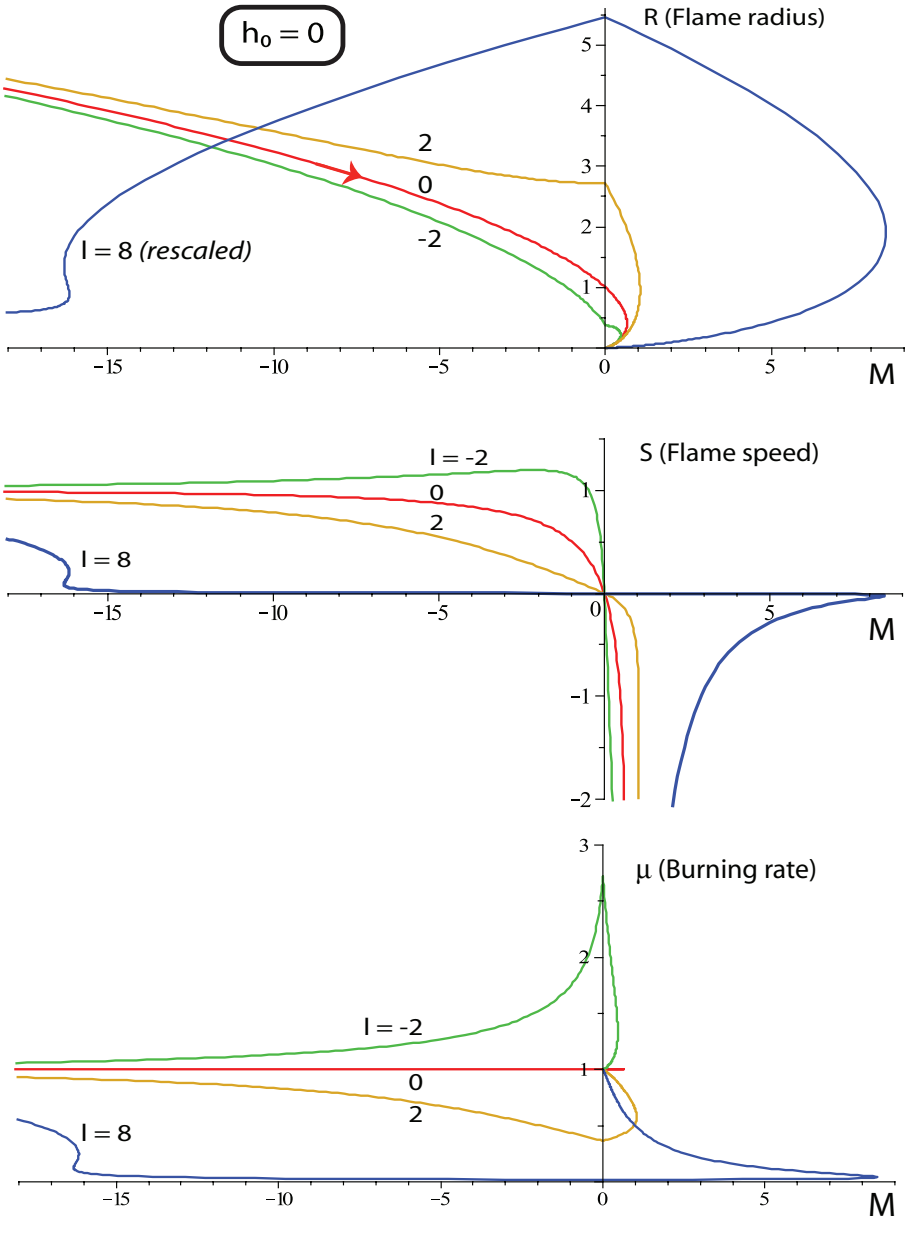

Figure 2. Flame radius R versus M (top), flame speed S versus M (middle) and burning rate per unit flame area μ versus M (bottom), for selected values of l. In the top subfigure, R is divided by 10 for the particular case $l = 8$; also an arrow has been added to the curve corresponding to $l = 0$ to indicate the direction of increasing m in the range $(-\infty, \infty)$.

When used with (17b), Equation (20) enables us to generate Figure 3. Plotted versus l are $M_{\max}$ (upper half-plane) and the values of M corresponding to the turning points of R versus M for $M < 0$ (curves in the lower half-plane). Four regions are thus delimited in the l-M plane, indicating the number of the stationary solutions. In the upper half plane, there are no solutions above the curve of $M_{\max}$ and two solutions below it. In the

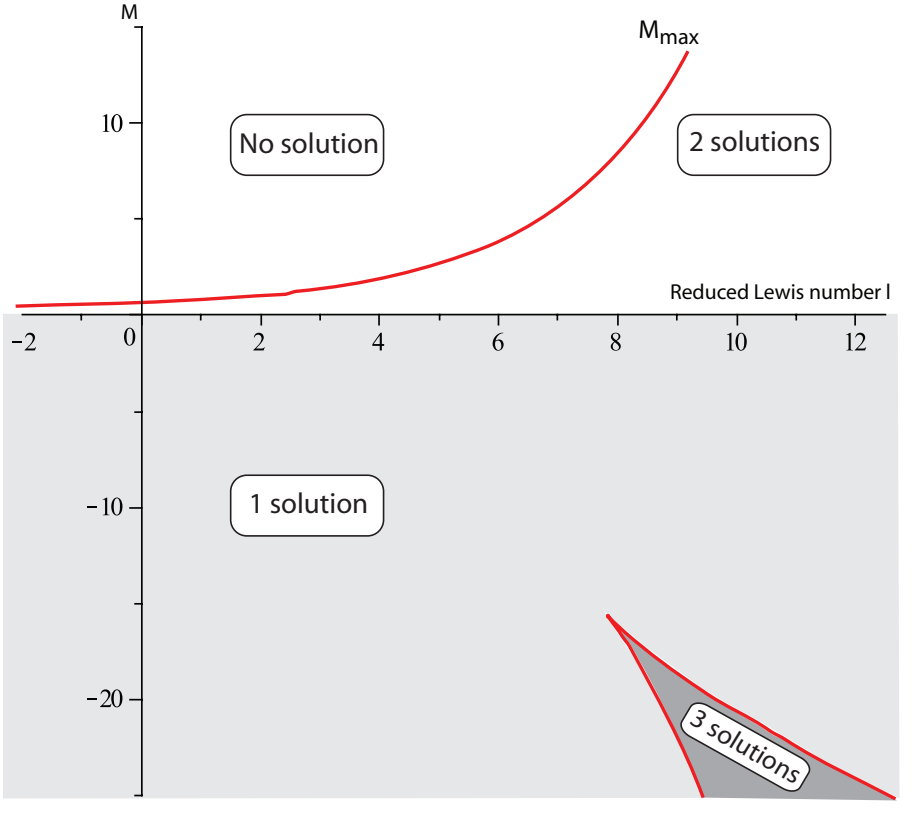

Figure 3. Maximum flow rate $M_{\max}$ allowing stationary solutions (curve in the upper half-plane), and the loci of the turning points of R versus M for $M < 0$ (curves in the lower half-plane).

lower half-plane, there is one solution, except in the cusp-region below the cusp, located at ($l_c = 7.83$, $M_c = -15.6$), approximately.

4.4. *Effect of h_0*

In this paragraph, we examine the effect of h_0 on the results, focusing our attention on the cases $M > 0$, since h_0 plays no part when $M \leq 0$; see also the Appendix. This effect is illustrated in Figure 4. Plotted is the flame radius R versus M for selected values of l, and three values of h_0 increasing from top to bottom. In the half-plane $M > 0$, all curves are inverse C-shaped passing through the origin, as found in the previous section. These curves shrink, with their tip located at the point $I \equiv (M_{\max}, R(M_{\max}))$ moving down and to the left, as h_0 increases or l decreases. As already hinted, I plays the role of an ignition point, and this fact will become clearer after the stability of the solutions is examined in Section 5. The results then indicate that ignition, defined as the transition from stationary to propagating flames, is more readily obtained for larger values of h_0 (i.e. hotter streams) and smaller values of l, since the source strength $M_{\max}$ needed for ignition is then smaller. This remark, which is in line with our physical expectation, is further confirmed in Figure 5, where $M_{\max}$ is plotted versus l for selected values of h_0.

Another way to examine the existence and multiplicity of the stationary solutions is to plot R versus l, for fixed values of M and h_0. This is carried out in Figure 6, using the fact that Equation (13) provides an explicit expression of l in terms of M, R and h_0.

The curves labelled $M = 0$ represent the classical Zeldovich flame balls. These curves and those corresponding to $M < 0$ are of course unaffected by the value of h_0. It can be seen that two branches of solutions exist for $M > 0$ provided that l is larger then a critical value $l_{\text{crit}}(M; h_0)$, depending on M and h_0. For each fixed value of h_0, these critical values generate a curve which is obviously identical to the curve of $M_{\max}$ versus l obtained for this particular value of h_0, as those in Figure 5.

4.5. *Flame speed and burning rate dependence on curvature*

An interesting feature of the current problem is that it provides analytically the flame speed S and the burning rate per unit flame area μ in terms of the flame curvature $\epsilon \equiv R^{-1}$, for all values of ϵ ranging from vanishingly small to infinitely large. Such analytical results may be valuable as a guide in interpreting the local behaviour of curved flames in more complex situations where analytical expressions are usually nonexistent, notably for highly

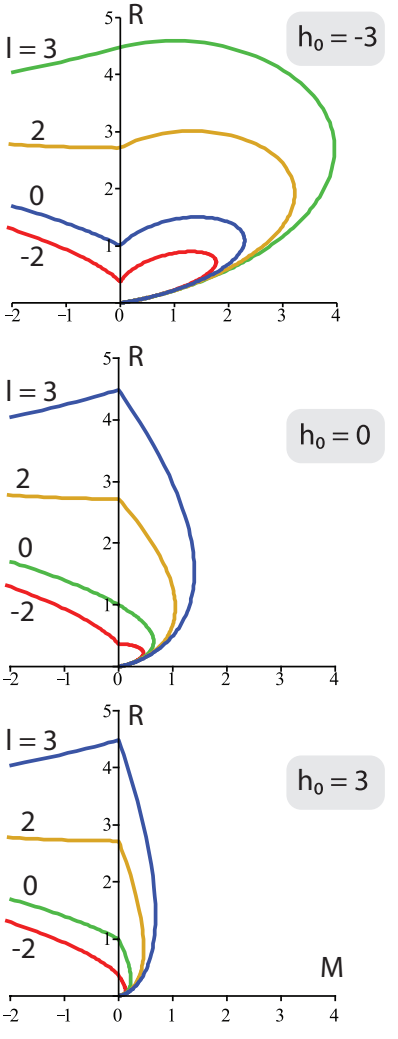

Figure 4. R versus M for selected values of l and $h_0 = -3$ (top), $h_0 = 0$ (middle), and $h_0 = 3$ (bottom).

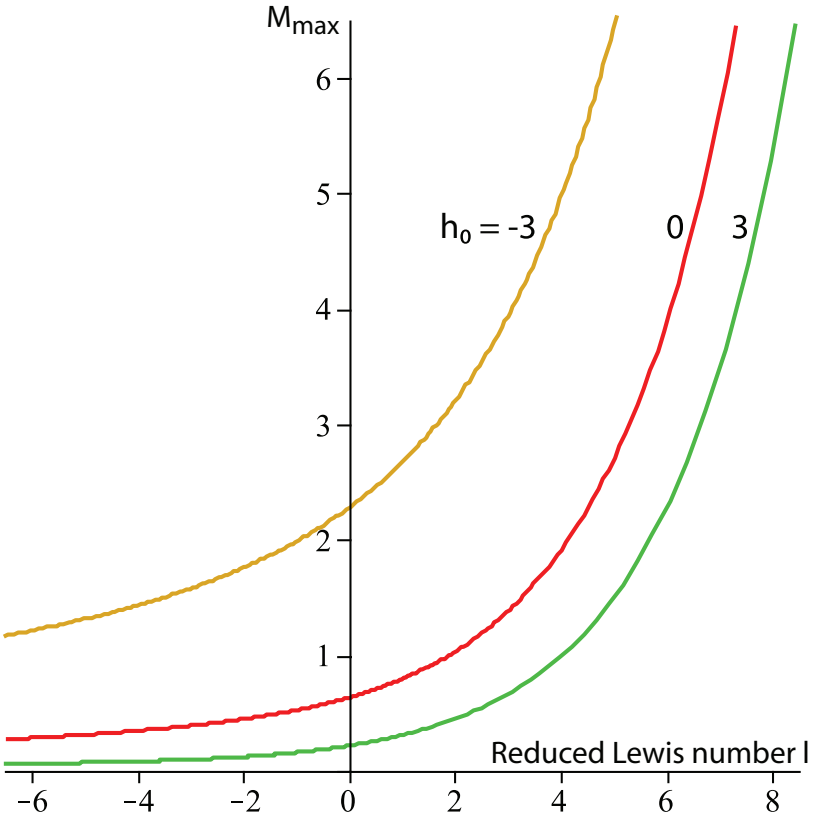

Figure 5. $M_{\max}$ versus l for selected values of h_0.

curved flames characterized by negative flame speeds. Examples of such situations include edge-flames in strained mixing layers referred to in the Appendix, and plausibly turbulent premixed flames.

More specifically, using Equations (14)–(17) and the fact that $m \equiv M/R = -S/\epsilon$, we obtain

$$\frac{S}{1-e^{-S/\epsilon}} = \exp\left\{\frac{l}{2}\frac{S/\epsilon}{1-e^{S/\epsilon}} + H(-S)\left[\frac{h_0}{2}(1-e^{S/\epsilon}) - \frac{l}{2}\frac{S}{\epsilon}\right]\right\}, \tag{21}$$

a formula which relates S to ϵ and involves the parameters l and h_0; this also determines μ which is given by either side of (21).

In the case of weakly curved flames, the flame properties approach those of the planar laminar flame, in particular, $S \to 1$ and $\mu \to 1$, in the limit $\epsilon \to 0$, as already indicated by the asymptotic results (18). The deviation of S and μ from their planar values due to the flame curvature are in fact negligible, transcendentally small, in the limit $\epsilon \to 0$, in agreement with available knowledge on weakly stretched flames [17]; the flame-stretch being zero for the stationary spherical flames under consideration.

In the case of highly curved flames, on the other hand, $S \to -\infty$ and $\mu \to \exp(h_0/2)$ in the limit $\epsilon \to \infty$, as indicated by the asymptotic results (19). More precisely, Equation (21) implies that

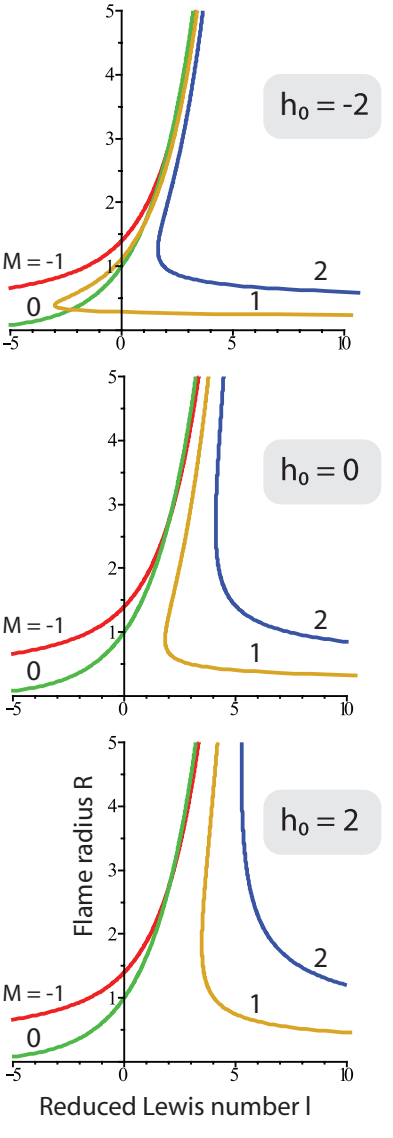

Figure 6. Flame radius R versus the reduced Lewis number l for selected values of M and $h_0 = -2$ (top), $h_0 = 0$ (middle), and $h_0 = 2$ (bottom).

$$S \exp \frac{S}{\epsilon} \sim -\mu \sim -\exp\left(\frac{h_0}{2} - \frac{l}{2\epsilon} \exp \frac{h_0}{2}\right) \qquad \text{as} \qquad \epsilon \to \infty\,, \tag{22}$$

a formula which clarifies the dependence of negative flame speeds S, and the corresponding burning rates μ, on large flame curvatures ϵ, and the parameters h_0 and l. We note that although the dependence of S on ϵ in (22) is not explicit, unlike that of μ, ϵ itself is an explicit function of S, namely $\epsilon = \left[S + \frac{l}{2} \exp\left(\frac{h_0}{2}\right)\right] / \left[\frac{h_0}{2} - \ln(-S)\right]$.

To close this section, we illustrate in Figure 7 the dependence of S and μ on ϵ, for selected values of l and $h_0 = -3$ (top), $h_0 = 0$ (middle), and $h_0 = 3$ (bottom). Concentrating first on the cases with $h_0 = 0$, we observe that negative burning speeds are only possible for

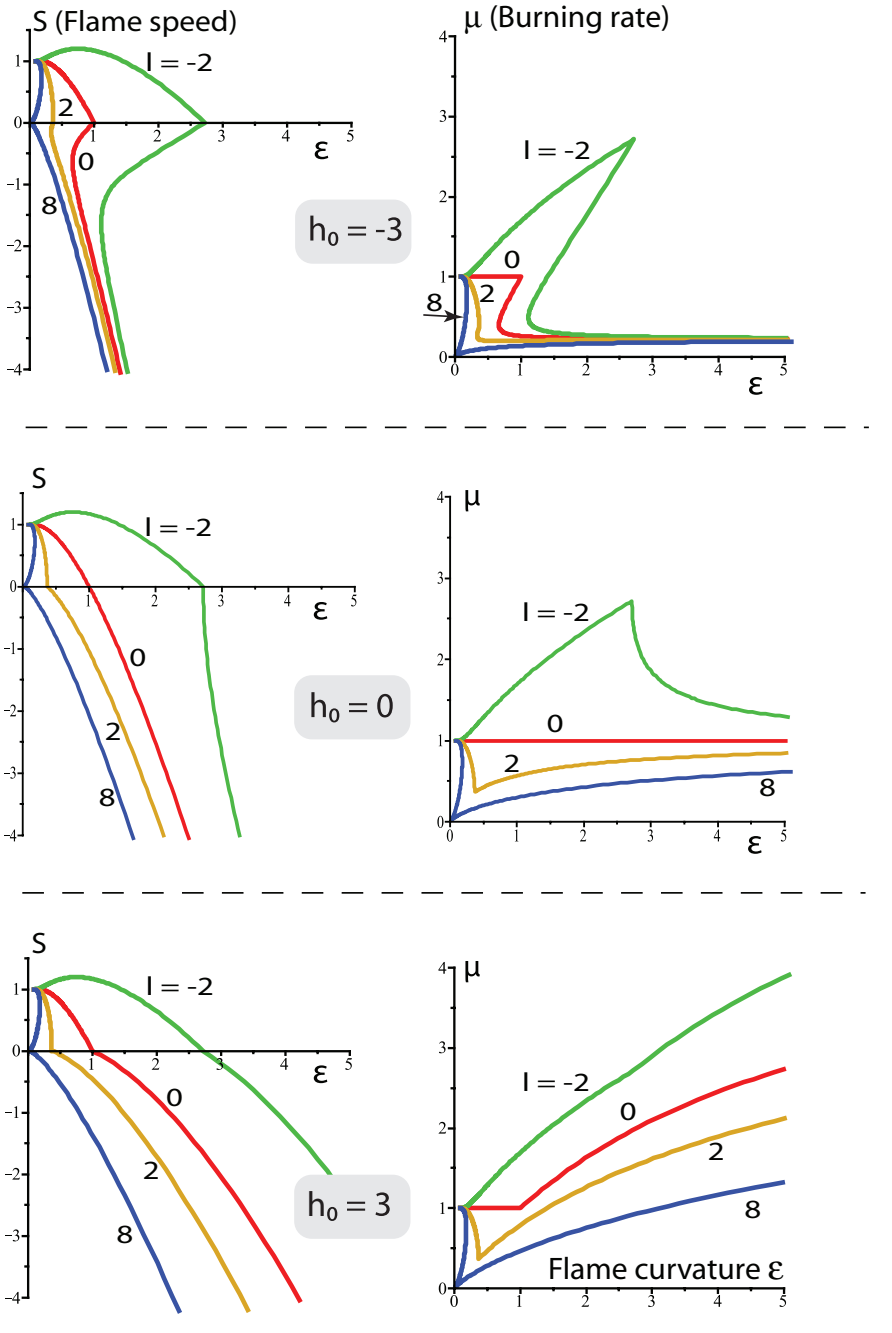

Figure 7. Flame speed S (left) and burning rate μ (right) versus flame curvature $\epsilon = R^{-1}$ for selected values of l and $h_0 = -3$ (top), $h_0 = 0$ (middle), and $h_0 = 3$ (bottom).

sufficiently large values of the flame curvature ϵ, except for sufficiently large values of the Lewis number. Typically, for moderate deviation of l from zero, S versus ϵ is single valued, and is monotonically decreasing for non-negative values of l. The burning rate μ on the other is constant for $l = 0$, and has typically a non-monotonic dependence on ϵ. We note

in particular that the location of the maximum of μ, for negative values of l, corresponds to the Zeldovich flame balls for which $S = 0$, and does not coincide with the location of the maximum of S.

The effect of h_0 on the results, more precisely on those corresponding to negative values of S, can be assessed by comparing the top, middle, and bottom figures. Beside the obvious fact that a decrease in the value of h_0 decreases both S and μ, it is observed that negative flame speeds and the corresponding burning rates may become typically multi-valued function of the flame curvature ϵ for $h_0 < 0$.

Finally, we note parenthetically that the relationships presented herein, relating the burning speed S or the burning rate μ to the flame curvature $\epsilon = R^{-1}$, can be nicely complemented by similar relationships pertaining to the well-studied problem of stationary spherical flames stabilized on a point source of Fuel. In the latter problem, the burning speed S cannot of course be negative, and, we have in fact $S = \mu$, if S is defined as the speed of the gas at the location of the reaction sheet. Without providing here the details of the derivation, we mention that the simple formula

$$S = \exp\left(\frac{h_\infty e^{-S/\epsilon}}{2}\right)$$

can be obtained, provided that the temperature θ_∞ of the ambient gas in the far field is close to unity (the adiabatic planar flame temperature) such that $h_\infty \equiv \beta(\theta_\infty - 1)$ is $\mathcal{O}(1)$ as $\beta \to \infty$. This formula is the counterpart of formula (21) and implies in particular that

$$S = 1 + EST \text{ as } \epsilon \to 0 \quad \text{and} \quad S \sim \exp\left(\frac{h_\infty}{2} - \frac{h_\infty}{2\epsilon}\exp\frac{h_\infty}{2}\right) \text{ as } \epsilon \to \infty\,.$$

5. Stability analysis

In this section, we carry out a linear stability analysis of the stationary solution $(\theta^0, h, r_f) = (\bar\theta, \bar h, R)$ given by (10), (11) and (13) by considering perturbed solutions of the form

$$r_f = R + \epsilon' e^{\sigma t}, \quad \theta^0 = \bar\theta + \epsilon' e^{\sigma t}\varphi(r), \quad h = \bar h + \epsilon' e^{\sigma t}\psi(r), \tag{23}$$

where r_f is the radius of the perturbed flame and ϵ' a small parameter characterizing the amplitude of the radial perturbations. By substitution into the equations and auxiliary conditions of Section 3, one ends up with $\varphi(r < r_f) \equiv 0$ and the equations

$$\varphi_{rr} + \frac{2r - M}{r^2}\varphi_r - \sigma\varphi = 0 \qquad (r > r_f) \tag{24}$$

$$\psi_{rr} + \frac{2r - M}{r^2}\psi_r - \sigma\psi = -l\sigma\varphi - \frac{lM}{r^2}\varphi_r \qquad (r \neq r_f) \tag{25}$$

subject to the boundary conditions

$$\varphi = 0, \qquad \psi = 0 \qquad \text{as} \quad r \to \infty \tag{26}$$

$$\begin{cases} \psi = 0 & \text{for} \quad M > 0 \\ \psi \text{ is bounded} & \text{for} \quad M \leq 0 \end{cases} \qquad \text{as} \quad r \to 0 \tag{27}$$

and the jump conditions

$$[\varphi] = -\mu\,, \qquad [\psi] = l\mu \tag{28a}$$

$$[\psi_r] + l[\varphi_r] = \frac{lM}{R^2}\mu \tag{28b}$$

$$[\varphi_r] = \left(\frac{\psi_*}{2} + \frac{2}{R} - \frac{M}{R^2} - H(M)\frac{M}{2R^2}(h_0 - h_*)\right)\mu \tag{28c}$$

at $r = R$. Here $\psi_* \equiv \psi(R_-)$, while $h_* \equiv h(R)$ and $\mu \equiv \exp(h_*/2)$ are given by (12) and (14), respectively.

It is to be noted that the jump conditions at the reaction sheet $r = r_f(t)$ have been transferred to $r = R$, using Taylor expansions about $r = R$, since $r_f - R$ is small, of $\mathcal{O}(\epsilon')$, according to (23)[4].

Equations (24)–(28) constitute an eigen-boundary value problem, whose solution should, in principle, provide a dispersion relation between the eigen values σ and the parameters of the problem of the form $F(\sigma; l, M, h_0) = 0$. This relation should determine whether a particular solution is stable or unstable, based on whether all perturbations of this solution have $Re(\sigma) < 0$ and thus decay, or at least one perturbation has $Re(\sigma) > 0$ and thus grows.

It is instructive to revisit first the particular case $M = 0$ pertaining to the classical Zeldovich flame balls, for which the dispersion relation can be determined analytically as known in the literature, see e.g. [1, p. 327]. Indeed, in this case, we have $h_* = -l$, $\mu = \exp(-l/2)$ and $R = \exp(l/2)$ on taking the limit $M \to 0$ in (12) and (13). Thus, the stability problem reduces to solving (24) to (27) with $M = 0$, along with the jump conditions $[\varphi] = -1/R$, $[\psi] = l/R$, $[\psi_r] + l[\varphi_r] = 0$, and $[\varphi_r] = \psi_*/2R + 2/R^2$ at $r = R = \exp(l/2)$. The solution satisfying all conditions, except the last jump condition, is given by

$$\varphi = \begin{cases} 0 & \text{if } r < R \\ \frac{1}{r}e^{(R-r)\sqrt{\sigma}} & \text{if } r > R \end{cases}$$

$$\psi = \begin{cases} \frac{l}{4r}\,\dfrac{e^{r\sqrt{\sigma}} - e^{-r\sqrt{\sigma}}}{e^{R\sqrt{\sigma}}} & \text{if } r < R \\ \frac{R}{r}e^{(R-r)\sqrt{\sigma}}\left\{\psi_* - \frac{l}{R}\left(1 + \frac{\sqrt{\sigma}}{2}(R-r)\right)\right\} & \text{if } r > R \end{cases}$$

with $\psi_* \equiv \psi(R_-) = l(e^{R\sqrt{\sigma}} - e^{-R\sqrt{\sigma}})/4Re^{R\sqrt{\sigma}}$, provided that we assume that $\mathrm{Re}(\sqrt{\sigma}) > 0$. The last jump condition then yields the dispersion relation

$$l = 4(R\sqrt{\sigma} - 1)(1 + \coth(R\sqrt{\sigma}))\,, \tag{29}$$

[4]More explicitly, Taylor expansions to $\mathcal{O}(\epsilon')$ yield the relations $[\varphi] = -[\bar{\theta}_r]$, $[\psi] = -[\bar{h}_r]$, $[\psi_r] + l[\varphi_r] = -[\bar{h}_{rr}] - l[\bar{\theta}_{rr}]$, and $[\varphi_r] = \left(\frac{\psi(R_-)}{2} + \frac{\bar{h}_r(R_-)}{2}\right)\exp\left(\frac{\bar{h}(R_-)}{2}\right) - [\bar{\theta}_{rr}]$, where the brackets designate jumps evaluated at $r = R$. These lead to the jump conditions (28) once the stationary solutions $\bar{\theta}$ and $\bar{h}$ given by (10) and (11) are used.

which implies that for any value of l there exists an unstable mode characterized by a value of σ which is real and positive[5]. Thus, we recover the known result that flame balls are always unstable, in the absence of other stabilizing effects, such as volumetric heat-losses, or the presence of a flow, $M \neq 0$, considered next.

Unfortunately, for $M \neq 0$, analytical derivation of a dispersion relation is not straightforward since, to start with, the general solution to (24) does not seem to be expressible in terms of familiar elementary functions, as it is the case when $M = 0$. To make progress we may turn into a numerical treatment, as done in the next section, where it is found in particular that the transition from stable to unstable behaviours, occurs without oscillations, thus suggesting that $\mathrm{Im}(\sigma) = 0$, and hence $\sigma = 0$, for marginal stability. We may also continue the analytical treatment but limiting our objective to determining the stability/instability domains in the l-M-h_0 space, without derivation of the dispersion relation itself. To this end, we look for marginal stability surfaces in the l-M-h_0 space by anticipating, as suggested by the numerics, that these are characterized by $\sigma = 0$. Thus, we solve (24) to (28) with $\sigma = 0$. The solution satisfying all conditions, except the last jump condition, is given by

$$\varphi = \begin{cases} 0 & \text{if } r < R \\ \mu \frac{1-e^{-M/r}}{1-e^{-M/R}} & \text{if } r > R \end{cases}$$

$$\psi = \begin{cases} \psi_* \left\{ 1 - H(M) \left(1 - \frac{e^{-M/r}}{e^{-M/R}} \right) \right\} & \text{if } r < R \\ \left(\psi_* + l\mu^2 R - l\mu \right) \frac{1-e^{-M/r}}{1-e^{-M/R}} - l\mu^2 \frac{R^2}{r} \frac{e^{-M/r}}{e^{-M/R}} & \text{if } r > R\,, \end{cases}$$

with

$$\psi_* = \frac{lM(R^{-1} - \mu)}{R(1 - e^{-M/R})[1 + H(M)M\mu^{-1}R^{-2}]}.$$

The last jump condition then yields a relation of the form $l = l(m; h_0)$, which turns out to be identical to Equation (20), valid at the turning points identified earlier. When this relation is used with Equation (17b) which is of the form $M = M(l; m, h_0)$, the marginal stability surfaces can be generated by varying the parameters m and h_0.

We conclude that, for a fixed value of h_0, the marginal stability curves coincide with the curves depicting the extremum values of M versus l, as shown in Figure 3, in the particular case $h_0 = 0$. Furthermore, since the solutions corresponding to the Zeldovich flame balls are unstable, any branch of solutions passing by these in Figure 4.3 (top) e.g. is unstable up to the turning points. In particular, in the domain $M > 0$ in Figure 3 where two solutions are found, the one with the larger radius is unstable, the one with the smaller radius stable; when $M < 0$ we are typically in the presence of a single solution which is unstable, except in the cusp region where three solutions exist, the middle one being stable, the others unstable. The picture is similar for $h_0 \neq 0$, since only the curve in the upper half plane in Figure 3 is shifted as h_0 is changed, as illustrated in Figure 5. The results are conveniently summarized in Figure 8, where four regions are delimited in the l-M-h_0 space, with the number of stationary solutions (flame balls) and their stability indicated in each region.

[5]This conclusion follows, e.g., from a plot of the simple explicit relation (29) of l versus the variable $R\sqrt{\sigma}$ assumed real and positive. Also, the assumption $\mathrm{Re}(\sqrt{\sigma}) > 0$ which has just been made is consistent with this conclusion.

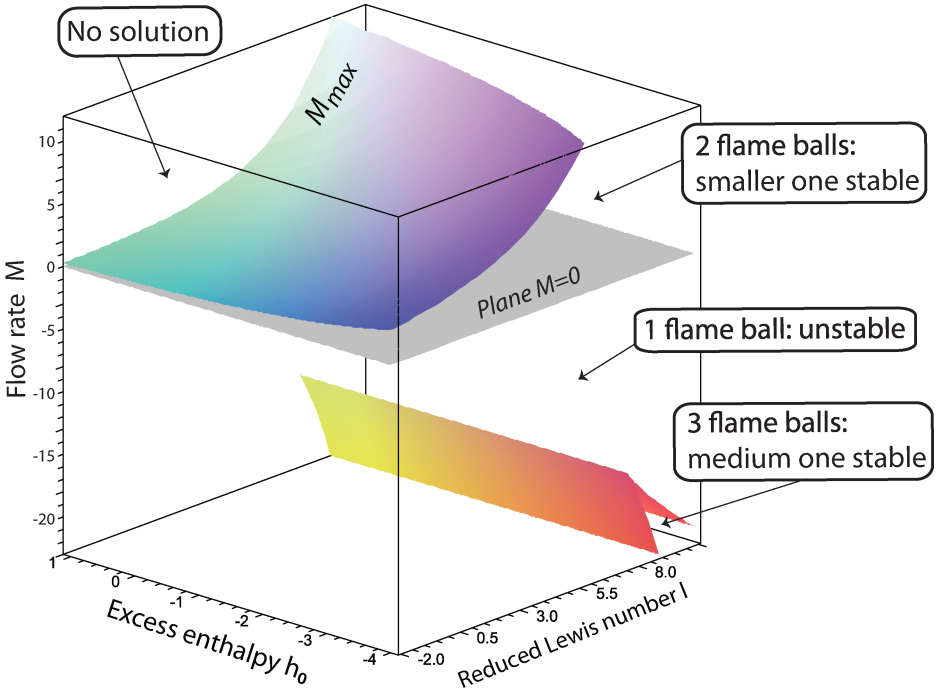

Figure 8. Number of stationary solutions (flame balls) and their stability in different regions of the l-M-h_0 space.

6. Numerical results

Although the analytical analysis performed in the asymptotic limit $\beta \to \infty$ is rather complete and self-contained, it is complemented here by a numerical study carried out with a finite value of β. As we shall see, this study confirms the analytical predictions, at least from the qualitative point of view, and provides further illustrations. More specifically, the problem defined by Equations (1)–(4) is solved numerically both as a time-dependent boundary value problem, with appropriate initial conditions, and as a stationary boundary value problem. A finite volume discretization in the space variable r is used to reduce the problem into a system of ordinary differential equations in the time-dependent case, and into a system of non-linear algebraic equations in the stationary case. The system of ordinary differential equations is solved by LSODA, a well tested robust solver with adaptive time-step which is suitable both for stiff and non-stiff problems [18]. The non-linear system of algebraic equations is solved with the NAG routine C05NBF [19], which is based on Powell's hybrid method [20]. The (non-dimensional) radial extent of the computational domain is typically from $r = 0$ to $r = 300$, with a non-uniform spatial-grid comprising 5000 points. A cutoff temperature $\theta_c = 0.01$ below which the reaction rate is set to zero is introduced to avoid the cold-boundary-difficulty. The values $\beta = 10$ and $\alpha = 0.85$ are adopted, with other parameters specified in each case.

6.1. *Stationary solutions*

Figure 9 shows the profiles of the temperature θ, the fuel mass fraction y_F, and the reaction rate ω (normalized by its maximum value $\omega_{\max}$) in an illustrative case corresponding to

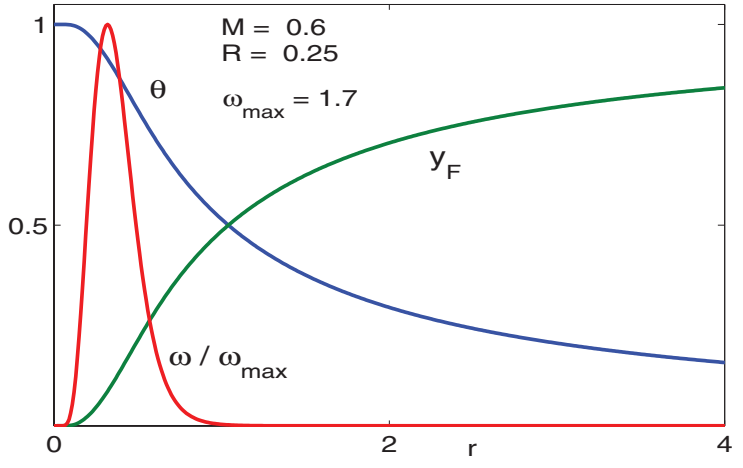

Figure 9. The profiles of the temperature θ, the fuel mass fraction y_F, and the normalized reaction rate $\omega/\omega_{\max}$ for $h_0 = 0$, $M = 0.6$ and Le $= 1$.

$M = 0.6$, $h_0 = 0$ and Le $= 1$. A flame ball of radius $R \approx 0.25$ is observed with this choice of parameters, R being defined as the location where the reaction rate is maximum.

A comparison between the analytical and numerical results is carried out in Figure 10 pertaining to $h_0 = 0$. Shown is the maximum flow rate $M_{\max}$ versus the Lewis number Le based on the numerics (solid curve) and the asymptotics (dashed curve). The agreement is excellent qualitatively, and good quantitatively provided the deviation of Le from unity are moderate, say Le in the range [0.6, 1.3].

The effect of h_0 is illustrated numerically in Figure 11 where R is plotted versus M, for selected values of h_0 and Le $= 1$. The results are in agreement with the asymptotics, with a single stationary solution obtained for $M < 0$, and two solutions for $M > 0$ less than a maximum value $M_{\max}$ which decreases with increasing h_0.

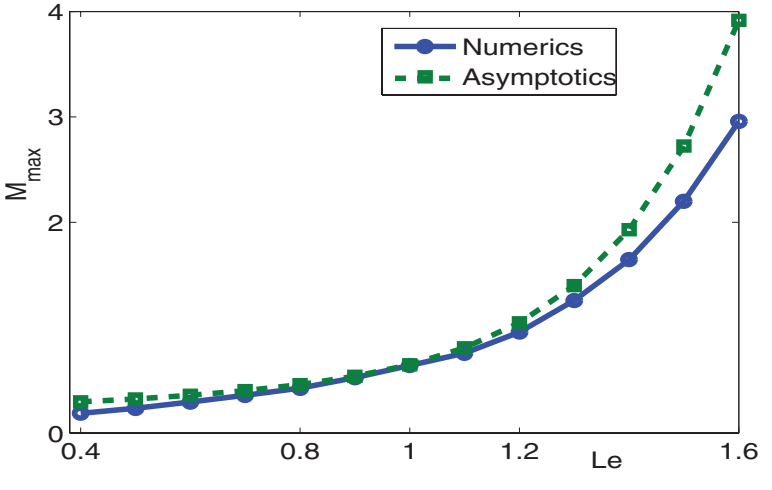

Figure 10. $M_{\max}$ versus Le for $h_0 = 0$ determined numerically (solid curve) and analytically (dashed curve).

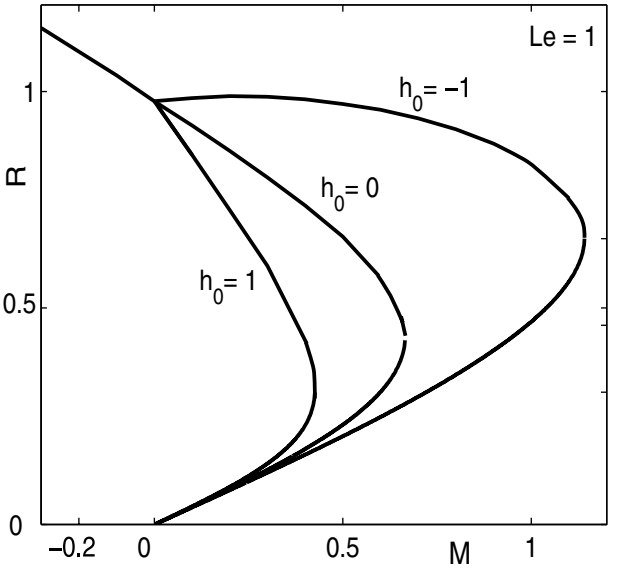

Figure 11. Flame radius R versus M for selected values of h_0 and Le $= 1$.

In addition to the multiplicity of solutions obtained for $M > 0$, multiple solutions are also predicted in the analytical study for $M < 0$ when Le is sufficiently larger than unity, as exemplified in Figure 4.3 (top subfigure, curve labelled $l = 8$). This fact is successfully confirmed numerically in Figure 12, where R is plotted versus M for Le $= 2$.

6.2. *Stability and time dependent calculations*

The stability of the stationary solutions to one-dimensional perturbations has been tested, using the following procedure. (1) The sparse non-linear algebraic problem is solved using the non-linear solver C05NBF to yield stationary solutions, each one being a vector with N

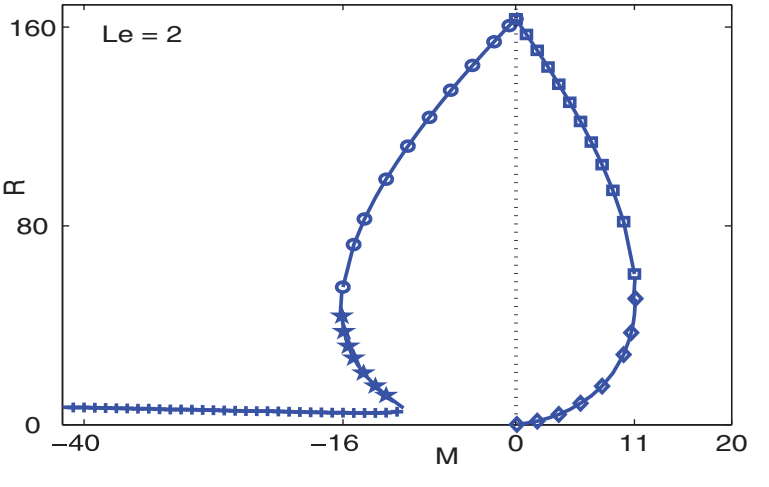

Figure 12. Flame radius R versus M for Le $= 2$. Stars (on the middle branch in the left half-plane) and diamonds (on the lower branch in the right half-plane) are computed solutions which are found stable.

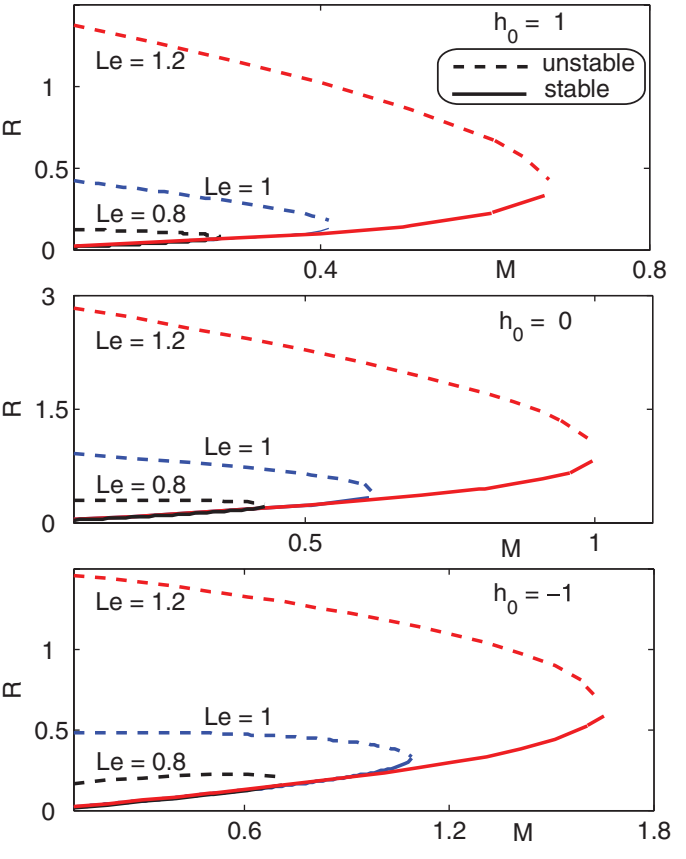

Figure 13. Flame radius R versus M for selected values of Le and $h_0 = 1$ (top), $h_0 = 0$ (middle), and $h_0 = -1$ (bottom). Solid lines represent branches of stable solutions and dashed lines branches of unstable solutions.

components, say $\underline{y}(N)$, N being twice the number of gridpoints. (2) Perturbations are added to the stationary solution $\underline{y}(N)$ to generate $\underline{y}^{\text{perturbed}}(N) = \underline{y}(N) + \epsilon \times \text{rand}(N)$, where $\epsilon = 10^{-4}$ and rand(N) an N-dimensional vector of random numbers from the standard normal distribution produced using the NAG routine G05FDF [19]. (3) The system of ODEs corresponding to the time-dependent problem is solved using LSODA, starting from the perturbed solution $\underline{y}^{\text{perturbed}}(N)$ as initial condition. When the resulting solution converges as time increases to a stationary solution $\underline{y}^*(N)$ such that $\|\underline{y}^*(N) - \underline{y}(N)\| < 10^{-5}$, the stationary solution $\underline{y}(N)$ is considered stable, otherwise unstable.[6]

By applying the testing procedure just described, we end up with the following conclusions. (a) When $M > 0$, the solutions represented by the upper branch of R versus M in Figure 13 are found to be unstable, while those represented by the lower branch stable. (b) When $M < 0$, no stable solutions were found except for values of the Lewis number well above one and for sufficiently large negative values of M where multiple solutions are obtained as illustrated in Figure 12 pertaining to Le $= 2$. The middle branch of the

[6]The notation $\|\cdot\|$ stands here for the maximum norm.

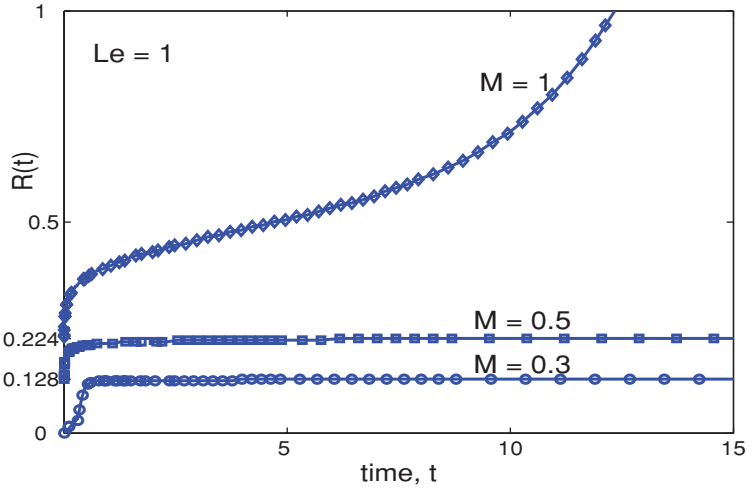

Figure 14. Flame radius R versus time t for selected values of M, with $h_0 = 0$ and Le $= 1$.

S-shaped curve in the left half-plane of this figure is found to be stable as predicted by the asymptotics, except in a small neighbourhood of the lower turning point (the stars on this branch indicate stable solutions[7]).

Finally, we carry out the following numerical experiment to illustrate the ignition process, i.e. the transition from stationary stable flame balls (lying on the lower branch of R versus M) to outwardly propagating flames, as M is increased. Starting with an initial condition corresponding to a frozen mixture, we simulate the blowing of hot air at the adiabatic flame temperature ($h_0 = 0$) with a flow rate $M = 0.3$. After a transient, the solution settles to a stationary flame ball with radius $R = 0.128$, as illustrated in Figure 14 where R is plotted versus time (curve labelled $M = 0.3$). Starting from this stationary solution as initial condition, the calculation is repeated with a higher value of $M = 0.5$; the radius of the ball increases to a new stationary value $R = 0.224$. Starting from this new stationary solution as initial condition, and repeating the computation with $M = 1$, it is seen that the flame radius continually increases with time, illustrating the transition from stationary to expanding spherical flames.

7. Conclusions

The problem under investigation has provided a complete analytical description of several fundamental aspects of combustion, made tractable by the simplifying assumptions of spherical symmetry and large activation energy. These aspects include the problem of ignition by a hot inert gas stream, the dependence of flame speeds, positive or negative, on the flame curvature, and the stability of the stationary solutions encountered which have been called generalized flame balls. In particular, as Zeldovich flame balls are used as criteria for successful ignition in stagnant reactive gases, generalized flame balls have been shown to provide similar criteria for ignition by a hot radial stream, a step towards understanding ignition by more practical flows of hot gases such as jets [12].

[7]We have checked that this small neighbourhood of the lower turning point with unstable solutions shrinks as β is increased (not shown here), improving thus the agreement with the asymptotics.

The main conclusions concerning the existence of generalized flame balls and their stability in the various regions of the l-M-h_0 space have been summarized in Figure 8: for $M \geq 0$ smaller than a maximum value $M_{\max}$ depending on l and h_0 two flame balls are found the smaller one being stable; for $M < 0$ we have typically a single solution which is stable unless the Lewis number Le is sufficiently greater than one and M has a sufficiently large negative value, in which case three flame balls exist the medium one being stable.

The ignition process has been discussed and illustrated in connection with Figure 14; typically if a hot gas is blown with a weak flow rate $M < M_{\max}$, a stable stationary flame ball forms, which increases in size as M increases, and generates an expanding flame ball when $M > M_{\max}$. This transition from stationary stable to propagating flames typifies successful ignition and presents strong similarities with flame initiation by a constant power heat-source in a stagnant environment described in [2].

Finally the dependence of the burning rate per unit flame area μ and the flame speed S on the flame curvature $\epsilon = R^{-1}$ has been described in Section 4.5 and Figure 7, and may provide insight when analysing the local behaviour of more complex flames such as turbulent premixed flames or edge-flames in mixing layers, where both positive and negative flame speeds are encountered.

Of course, the results established within our simple model can be extended in future studies to account for several additional effects, such as the size of the source (which has been modelled as a point-source in this paper), the presence of heat-losses coupled with the flow, a non-spherical geometry, etc.

References

[1] Ya. Zeldovich, G. Barenblatt, V. Librovich, and G. Makhviladze, *The Mathematical Theory of Combustion and Explosions*, Consultants Bureau, New York, 1985.

[2] B. Deshaies and G. Joulin, *On the initiation of a spherical flame kernel*, Combust. Sci. Technol. 37 (1984), pp. 99–116.

[3] J. Buckmaster, G. Joulin, and P. Ronney, *The structure and stability of nonadiabatic flame balls*, Combust. Flame 79 (1990), pp. 381–392.

[4] J. Buckmaster, G. Joulin, and P. Ronney, *The structure and stability of nonadiabatic flame balls: the effects of far-field losses*, Combust. Flame 84 (1991), pp. 411–422.

[5] G. Joulin and J.D. Buckmaster, *Influence of boundary losses on structure and dynamics of flame-balls*, Combust. Sci. Technol. 89 (1993), pp. 57–69.

[6] J. Buckmaster and G. Joulin, *Flame balls stabilized by suspension in fluid with a steady linear ambient velocity distribution*, J. Fluid Mech. 227 (1991), pp. 407–427.

[7] P. Ronney, *Near-limit flame structures at low Lewis number*, Combust. Flame 82 (1990), pp. 1–14.

[8] P. Ronney, M. Wu, H. Pearlman, and K. Weiland, *Experimental study of flame balls in space: preliminary results from STS-83 space flight experiments*, AIAA J. 36 (1998), pp. 1361–1368.

[9] G. Joulin, *Point-source initiation of lean spherical flames of light reactants – an asymptotic theory*, Combust. Sci. Technol. 43 (1985), pp. 99–113.

[10] M. Champion, B. Deshaies, G. Joulin, and K. Kinoshita, *Spherical flame initiation: theory versus experiments for lean propane-àair mixtures*, Combust. Flame 65 (1986), pp. 319-337.

[11] F.A. Williams, *Combustion Theory* ,Benjamin-Cummings, Menlo Park, CA, 1985.

[12] R. Sadanandan, D. Markus, R. Schießl, U. Maas, J. Olofsson, H. Seyfried, M. Richter, and M. Aldén, *Detailed investigation of ignition by hot gas jets*, Proc. Combust. Inst. 31 (2007), pp. 719–726.

[13] J.D. Buckmaster and G.S.S. Ludford, *Lectures on Mathematical Combustion*, Society for Industrial and Applied Mathematics, Philadelphia, 1983.

[14] C. Lee and J. Buckmaster, *The structure and stability of flame balls: a near-equidiffusional flame analysis*, SIAM J. Appl. Math. 51 (1991), pp. 1315–1326.

[15] G. Joulin and P. Vidal, *Hydrodynamics and Nonlinear Instabilities*, Cambridge University, Cambridge, 1998.
[16] J.H. Tien and M. Matalon, *On the burning velocity of stretched flames*, Combust. Flame 84 (1991), pp. 238–248.
[17] M. Matalon, *On flame stretch*, Combust. Sci. Technol. 31 (1983), pp. 169–181.
[18] A. Hindmarsh, *ODEPACK: A systematized collection of ODE solvers*, in R.S. Stepleman et al., eds., *Scientific Computing*, North Holland, New York, 1983, pages 55–64.
[19] Numerical Algorithms Group (NAG), *Fortran Library Mark 20*, Oxford, 2001.
[20] M. Powell, *A hybrid method for nonlinear algebraic equations*, in P. Rabinowitz, ed., *Numerical Methods for Nonlinear Algebraic Equations*, Gordon and Breach, New York, 1970.
[21] J. Daou and A. Liñán, *The role of unequal diffusivities in ignition and extinction fronts in strained mixing layers*, Combust. Theory Model. 2 (1998), pp. 449–477.
[22] J. Daou and A. Liñán, *Ignition and extinction fronts in counterflowing premixed reactive gases*, Combust. Flame 118 (1999), pp. 479–488.

Appendix: A special class of solutions

There is a fundamental change in the character of the generalized flame balls described in this paper as M varies from negative to positive values. Namely, while h (and hence the temperature θ) is constant in the burnt gas for $M \leq 0$, it is typically dependent on r and the enthalpy at the source h_0 when $M > 0$, as implied by the boundary condition (8). We note however from (11) and (12) that the special choice $h_0 = -lM/R(1 - e^{-M/R})$ when $M > 0$ leads to the constancy of h inside the ball, as for the cases $M \leq 0$. The solutions with constant h in the burnt gas can be thus viewed as stationary solutions to a problem depending on the two parameters M and l, which is defined by Equations (5) and (6) applied in the domain $r > r_f$, along with the requirements $\theta^0(r < r_f) = 1$ and $h(r < r_f) = \text{const}$, the far-field boundary condition (7) and the jump conditions (9). The solutions corresponding to $M = 0$ of this two-parameter problem (i.e. Zeldovich flame balls) can be extended smoothly to positive and negative values of M, unlike the solutions to the three-parameter problem discussed above, which are typically continuous but non-smooth functions of M as $M \to 0$. Of course, although the two-parameter problem is simpler to study than the three-parameter problem, its solutions are more difficult (but conceptually possible) to obtain experimentally, requiring a special choice of h_0. The object of this appendix is to present briefly the main results of this simpler, albeit less realistic, model.

As before, stationary solutions satisfying all equations except the last jump condition 9c are readily determined, and are given by

$$\theta^0 = \begin{cases} 1 & \text{for} \quad r \leq R \\ \frac{1-e^{-M/r}}{1-e^{-M/R}} & \text{for} \quad r \geq R \end{cases} \tag{30}$$

$$h = \begin{cases} -\frac{lM}{R}\frac{1}{1-e^{-M/R}} & \text{for} \quad r \leq R \\ -\frac{lM}{R}\frac{1-e^{-M/r}}{1-e^{-M/R}} - \frac{lM}{r}\frac{e^{-M/r}}{1-e^{-M/R}} & \text{for} \quad r \geq R. \end{cases} \tag{31}$$

Using these solutions in (9c), we obtain

$$\frac{M}{R^2}\frac{e^{-M/R}}{1-e^{-M/R}} = \exp\left(-\frac{lM}{2R}\frac{1}{1-e^{-M/R}}\right), \tag{32}$$

which allows the flame ball radius R to be determined in terms of M and l; in the particular case $M = 0$ pertaining to Zeldovich flame balls, a Taylor expansion for small M provides $R = \exp(l/2)$, as found in the literature [15, p. 530].

Also the effect of M on the flame radius R is easily obtained by recasting Equation (32) into the form

$$R = R(m;l) = \frac{m \exp\left(\frac{l}{2}\frac{m}{1-e^{-m}}\right)}{e^m - 1}, \qquad M = M(m;l) = mR(m,l) \tag{33}$$

involving the parameter $m \equiv M/R$. This allows parametric plots of R versus M for selected fixed values of l to be generated as in Figure 15. Since there is no difference between the three- and two-parameter models for $M \leq 0$, we emphasize in this appendix only the case $M > 0$. In particular, we note that in the limit $m \to \infty$, we have $R \to 0$ and $M \to 0$ *only if* $l < 2$ and $R \to \infty$ and $M \to \infty$ if $l \geq 2$; this explains the disappearance of the lower branch containing the origin for $l = 2$ (or larger values, which are not shown). Thus $l = 2$ appears as a critical value below which the curves of R versus M are multi-valued, and above which they are single-valued. In the multi-valued cases corresponding to $l < 2$, two solutions are typically present for positive values of M, provided that M is smaller than a maximum value $M_{\max}$ depending on l which characterizes the turning points in Figure 15. The curve depicting $M_{\max}$ versus l, given in Figure 16, shows that M increases with l and tends to infinity as $l \to 2$. In the domain above this curve there are no solutions; in the domain below it, delimited by the vertical line $l = 2$ and the horizontal line $M = 0$, two flame balls exit; everywhere else in the l-M domain, including in the half-plane $M < 0$ (which is not shown), a single flame ball exists except outside the cusp region in Figure 3. Also, using Equation (32), we can plot R versus l for fixed values of M, as shown in Figure 17, where the curve labelled $M = 0$ represent Zeldovich flame balls, for which $R = \exp(l/2)$.

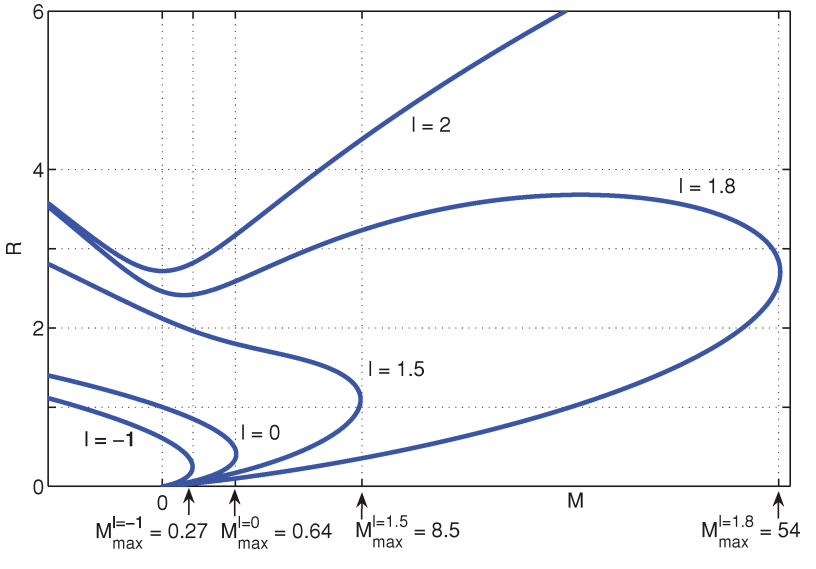

Figure 15. R versus M for selected values of l.

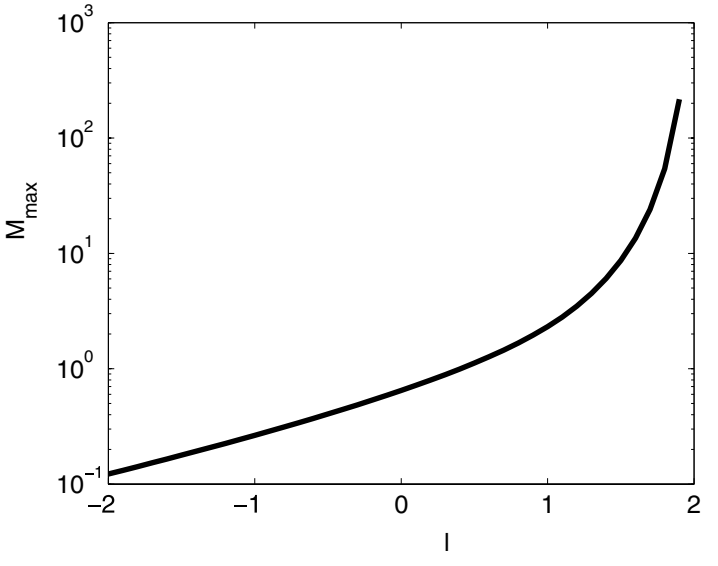

Figure 16. M_{max} versus l.

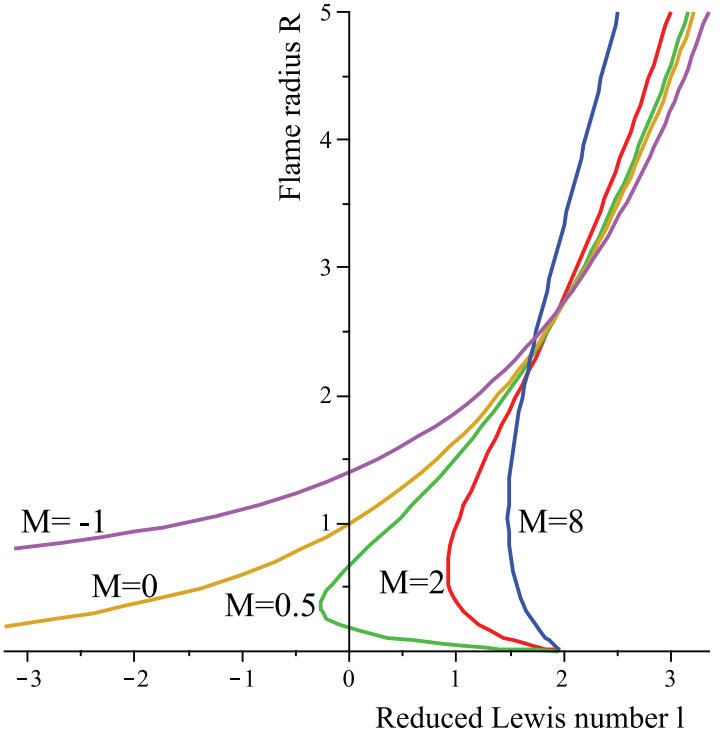

Figure 17. R versus l for selected values of M.

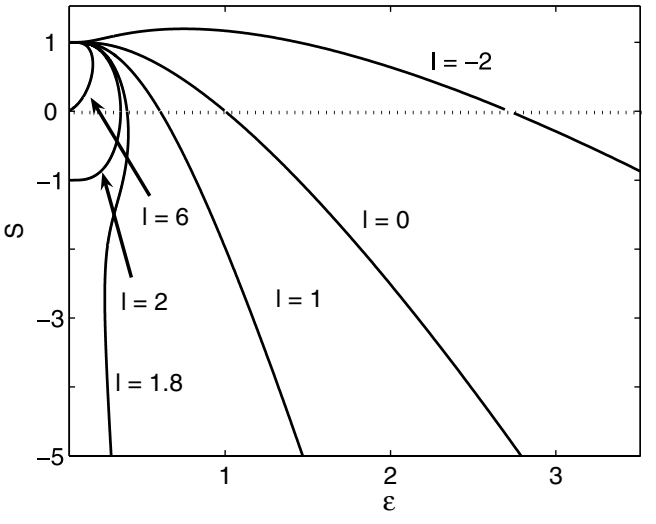

Figure 18. Flame speed S versus $\epsilon = R^{-1}$ for selected values of l.

Finally, a plot of the flame speed S versus the flame curvature $\epsilon = R^{-1}$ is provided for selected values of l in Figure 18, and can be compared with Figure 7 pertaining to the three-parameter model. We note that the range of flame curvatures ϵ and the range of negative speeds S cannot be arbitrarily large if $l \geq 2$ within the two-parameter model. However, the transition from positive to negative speeds occurs now smoothly as ϵ is increased. Furthermore, the curves plotted nicely mimic, when $l < 2$, the numerically observed variation of the propagation speed of edge-flames with a strain-related parameter ϵ determining their curvatures (compare with Figure 3 in [21] and Figure 6 in [22]).